iScience

CellPress
OPEN ACCESS

Article

Controllable preparation and performance of bio-based poly(lactic acid-iminodiacetic acid) as sustained-release Pb^{2+} chelating agent

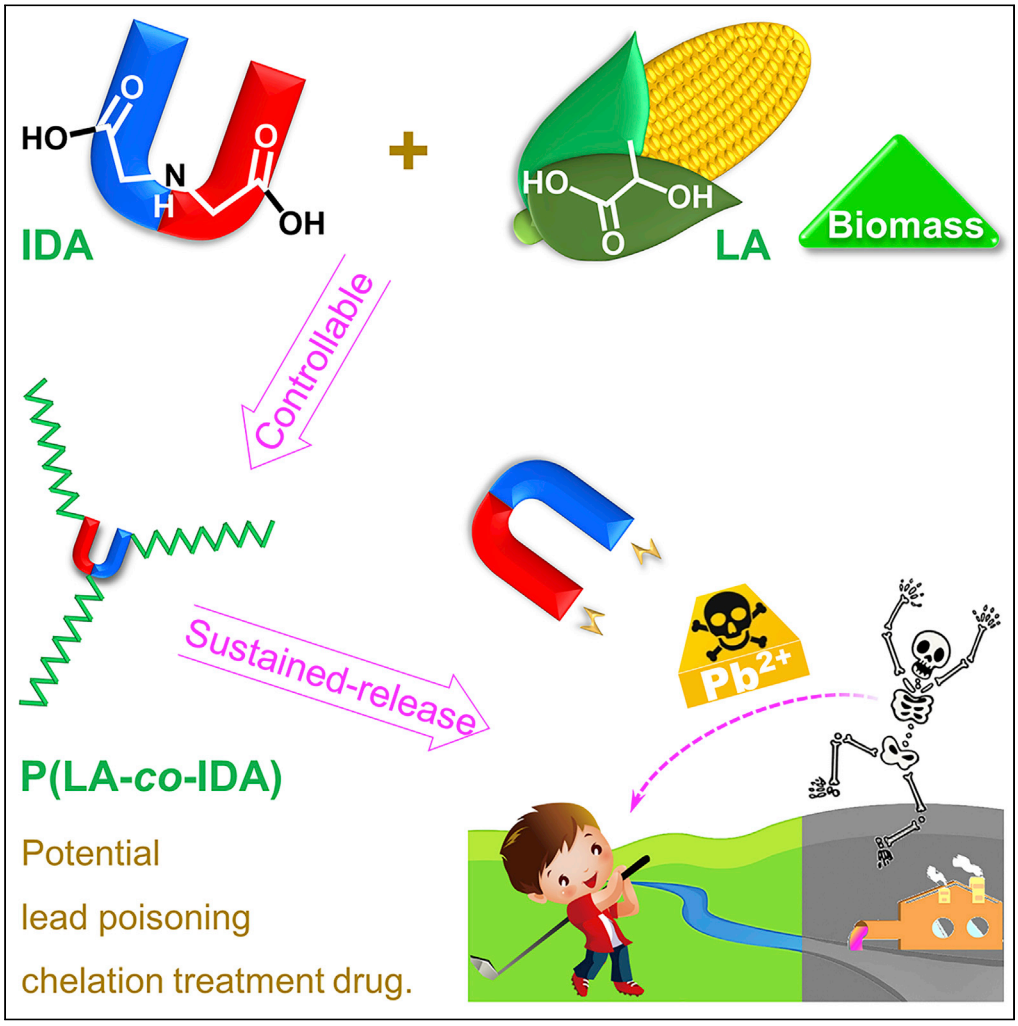

Jian-Yun Lin, Xi-Ying Cao, Ying Xiao, ..., Li-Ting Yang, Yong-Gan Fang, Zhao-Yang Wang

pinky_r@163.com (S.-H.L.)
yanglt@scnu.edu.cn (L.-T.Y.)
wangzy@scnu.edu.cn (Z.-Y.W.)

Highlights

Novel bio-based polymeric Pb^{2+} chelating agent is first developed from lactic acid

The star-shaped structure and properties of P(LA-*co*-IDA) can be controlled by DMP

The products can be sustainably degraded and released to chelate Pb^{2+} as designed

Tunable Pb^{2+} chelating capacity is suitable for drug in lead poisoning treatment

Lin et al., iScience *24*, 102518
June 25, 2021
https://doi.org/10.1016/j.isci.2021.102518

iScience

CellPress
OPEN ACCESS

Article

Controllable preparation and performance of bio-based poly(lactic acid-iminodiacetic acid) as sustained-release Pb^{2+} chelating agent

Jian-Yun Lin,[1] Xi-Ying Cao,[1] Ying Xiao,[1] Jin-Xin Wang,[1] Shi-He Luo,[1,2,*] Li-Ting Yang,[1,*] Yong-Gan Fang,[1] and Zhao-Yang Wang[1,2,3,*]

SUMMARY

The bio-based lactic acid (LA) and the common metal ion chelating agent iminodiacetic acid (IDA) are used to design and prepare a polymeric sustained-release Pb^{2+} chelating agent by a brief one-step reaction. After the analysis on theoretical calculation for this reaction, poly(lactic acid-iminodiacetic acid) [P(LA-*co*-IDA)] with different monomer molar feed ratios is synthesized via direct melt polycondensation. P(LA-*co*-IDA) mainly has star-shaped structure, and some of them have two-core or three-core structure. Thus, a possible mechanism of the polymerization is proposed. The degradation rate of P(LA-*co*-IDA)s can reach 70% in 4 weeks. The change of IDA release rate is consistent with the trend of the degradation rate, and the good Pb^{2+} chelating performance is confirmed. P(LA-*co*-IDA) is expected to be developed as a lead poisoning treatment drug or Pb^{2+} adsorbent in the environment with long-lasting effect, and this research provides a new strategy for the development of such drugs.

INTRODUCTION

Sustainable development has always been an important issue for humans (Naidoo and Fisher, 2020) along with material sustainability requiring the integration of green chemistry and raw material development (Zimmerman et al., 2020), especially the full utilization of renewable raw materials (Stockmann et al., 2020). Owing to the irreversibility constraint of the materials from petrochemical resources (Giraud et al., 2020), making use of biomass, the most abundant renewable carbon feedstock in the world (Liao et al., 2020) as an important way to the circular sustainable economy (Faveere et al., 2020) has great potential to replace or even surpass petrochemical feedstocks in most cases (Wang et al., 2020a, 2020b). Bio-based materials derived from biomass have been proved to be applicable to vaccine carriers (Fruk et al., 2021), electronic products (Maiti et al., 2019), industrial products (Hu et al., 2020), daily necessities (Chen et al., 2020), fuels (Sherkhanov et al., 2020), and many other fields (Byun and Han, 2020). Among them, polylactic acid (PLA), as the most widely used bio-based polymer (Hermann et al., 2020), has been recognized by the US Food and Drug Administration because of its good biocompatibility (Massoumi et al., 2020; Shin et al., 2019) and biodegradability (Luo et al., 2017; He et al., 2019a, 2019b). And the functionalization of PLA materials has attracted great attention in the fields of biomedicine (Wang et al., 2020a, 2020b), packaging (Calvino et al., 2020), and 3D printing (Silva Vinicius et al., 2020). Even so, there is still an urgent need to develop more ecological technologies and green products in some important areas.

Despite the global environmental regulations becoming stricter, heavy metals still pose a serious threat to human health (Fry et al., 2020). Among them, Pb^{2+} enters the human body extremely easily in people's daily life and work (Puangprasert and Prueksasit, 2019) and can be deposited in the blood, soft tissue, and bone, leading to the damage of various organ systems (Srivats et al., 2020), especially the irreversible neurodevelopmental disorders in children. Therefore, lead poisoning is a global public health problem that needs urgent solution (Yan et al., 2020). Pb^{2+} in human body is usually excreted after chelation by dimercaptopropanol or other drugs, to reduce its absorption, accumulation, and toxicity (Srivats et al., 2020). However, the traditional small molecule-type chelating agents have obvious disadvantages, such as large dosage, high toxicity, and non-biodegradation (Bretti et al., 2017; He et al., 2019a, 2019b). Thus, it is of great practical significance to develop polymeric chelators with biocompatibility, biodegradability, and long-term efficacy

[1]School of Chemistry, South China Normal University, Key Laboratory of Theoretical Chemistry of Environment, Ministry of Education, Guangzhou Key Laboratory of Analytical Chemistry for Biomedicine, Guangzhou 510006, P. R. China

[2]Key Laboratory of Functional Molecular Engineering of Guangdong Province, School of Chemistry and Chemical Engineering, South China University of Technology, 381 Wushan Road, Guangzhou 510640, P. R. China

[3]Lead contact

*Correspondence: pinky_r@163.com (S.-H.L.), yanglt@scnu.edu.cn (L.-T.Y.), wangzy@scnu.edu.cn (Z.-Y.W.)

https://doi.org/10.1016/j.isci.2021.102518

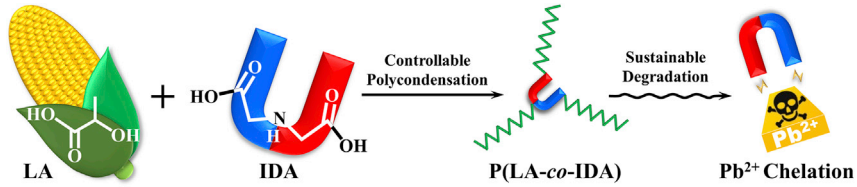

Scheme 1. Synthesis, degradation, and Pb^{2+} chelation of P(LA-*co*-IDA)

(Tahtat et al., 2017; Bretti et al., 2019). As far as we know, to date, there have been no reports on such chelating agents based on PLA materials.

As a polycarboxylic acid with a secondary amino group, iminodiacetic acid (IDA) has good biocompatibility (Zou et al., 2017). As its lone pair electrons on O atom in carboxyl group can be shared with the empty orbital of metal ion to form a stable coordination compound (Zhou et al., 2018), IDA has been widely used as a chelating agent in industrial (Lin et al., 2018; Amphlett et al., 2018; Anito et al., 2020) and biomedical fields (Gokcal et al., 2020). As a bio-based and renewable hydroxycarboxylic acid (Lin et al., 2021), lactic acid (LA) is the basic monomer for the synthesis of PLA and can be copolymerized with many different functional monomers to prepare the multifunctional PLA materials (Oh et al., 2020). Herein, for the first time, a new copolymer poly(lactic acid-iminodiacetic acid) [P(LA-*co*-IDA)] is briefly synthesized from IDA and LA by simple direct melt polycondensation (Scheme 1) and successfully used as a chelating agent for Pb^{2+}.

RESULTS AND DISCUSSION

In this study, IDA is used as a multifunctional reagent containing a secondary amino group and two carboxyl groups for the copolymerization with LA. In theory, they can form not only linear copolymer (Scheme 2) but also star copolymer, and even multi-core non-linear copolymers (Scheme 3). Therefore, the energy barriers of esterification reaction (the first step for forming linear copolymer) and amidation reaction (the first step for forming non-linear copolymer) of LA and IDA were first compared by theoretical calculation. Then, on the basis of the analysis for the calculation results, the polymerization conditions were screened, and the structure and physical properties of the obtained products were characterized. Importantly, the effects of *n*(LA):*n*(IDA) on the structure and Pb^{2+} chelating properties of P(LA-*co*-IDA) were systematically explored.

Theoretical calculation and analysis

As per the reported method, (Ayers and Parr, 2000; Ye and Neese, 2011; Ortega et al., 2020), the Fukui function charge distribution value of atoms in LA and IDA molecules are shown in Tables S1 and S2 and the highest occupied molecular orbital (HOMO) and the lowest unoccupied molecular orbital (LUMO) of LA and IDA molecules are shown in Figures S1 and S2, respectively. According to the frontier orbital theory, the Fukui(−) and Fukui(+) value of atoms can be used to quantitatively characterize their electrophilic and nucleophilic reaction activities, respectively. The larger the value is, the more likely it is to be the active site of the corresponding reaction type (Ayers and Parr, 2000). From Table S1 and Figure S1, the O atom (O-2) of hydroxyl in LA molecule is the active site for electrophilic reaction, whereas the C atom (C-4) of carboxyl is the active site for nucleophilic reaction. From Table S2 and Figure S2, the N atom (N-4) of secondary amino group in IDA molecule is the active site for electrophilic reaction, whereas the carboxyl C atoms (C-2 and C-6) are the active sites for nucleophilic reaction.

HOMO has a weaker binding force to electrons, showing the property of donating electron in the reaction. E_{HOMO} represents the electron-donating ability of a molecule: the larger the value, the stronger the electron-donating ability of the molecule. LUMO has a stronger affinity for electrons, having the property of an electron acceptor. E_{LUMO} represents the electron-withdrawing ability of a molecule: the smaller the value, the stronger the electron-withdrawing ability of the molecule (Lu and Manzetti, 2014; Wang et al., 2021). Therefore, when only the esterification reaction occurs between LA and IDA, the hydroxyl O-2 of LA initiates nucleophilic attack on the carboxyl C-2 and C-6 of IDA, and water molecules are removed to form ester bonds, then the linear P(LA-*co*-IDA) copolymer can be generated (Scheme 2). When both esterification and amidation reaction occur between LA and IDA, carboxyl C-4 of LA can launch an electrophilic attack against secondary amino N-4 of IDA also removing water molecules to form amide bond. Thus, the star-shaped P(LA-*co*-IDA) may be generated directly from LA and IDA (Scheme 3), or indirectly from two monomers via the linear copolymer (Scheme 4). Furthermore, these non-linear P(LA-*co*-IDA)s with multi-core structure also can be generated (Scheme 3).

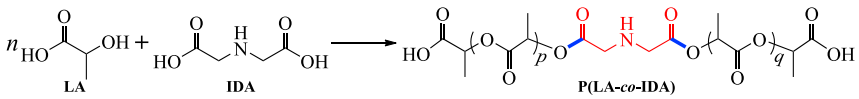

Scheme 2. Synthesis of linear P(LA-*co*-IDA)

To compare the difficulty in directly producing linear and star-shaped P(LA-*co*-IDA)s, the transition states of LA-IDA bimolecular esterification and amidation reaction were searched by chemical calculation (Ortega et al., 2020); the results are shown as Figures 1 and S3, respectively. It can be seen that the reaction energy barrier of the esterification reaction is 46.177 kcal·mol^{-1} and the value for the amidation reaction is 87.386 kcal·mol^{-1}. Although the latter is higher than the former indeed, the gap between them is not particularly large (Gorantla and Mallik, 2020; Roytman and Singleton, 2020). In fact, there are a large number of reports showing that the secondary amino group in IDA can react with carboxyl (Charton et al., 2015; Suda et al., 2006), ester group (Suda et al., 2006), epoxy group (Lin et al., 2018; An et al., 2017), acyl chloride (Charton et al., 2014, 2015), or anhydride (Leydier et al., 2012) to form amide group. In addition, imposing the appropriate reaction conditions can facilitate to cross the reaction barrier (Torres et al., 2020). Therefore, by screening the reaction conditions, such as the molar feed ratio *n*(LA): *n*(IDA), catalyst type, catalyst dosage, reaction temperature, and reaction time, it is possible to control the structure of P(LA-*co*-IDA).

Screening for synthetic conditions

The synthetic conditions were explored by selecting different influence factors at the molar feed ratio of *n*(LA): *n*(IDA) = 32 : 1, such as catalyst type and dosage, polymerization temperature and time, and according to the principle that the entry with the largest intrinsic viscosity of the copolymer P(LA-*co*-IDA) is the best (Wang et al., 2006, 2011). The screening results are shown in Table 1.

Catalyst seriously affects the performance, yield, and appearance of the product (Yuntawattana et al., 2020). It can be seen from Table 1 that the P(LA-*co*-IDA) synthesized by using SnO as catalyst has the highest intrinsic viscosity and relatively high yield, and its appearance is like white powder. These indicate that SnO catalyst is necessary and optimal (**Entries 1–5**), and suitable for use in subsequent experiments. At the same time, with the increase of the catalyst dosage (**Entries 6–10** versus **Entry 2**), although all products are white powder, the intrinsic viscosity of the products is generally increased first and then decreased. Obviously, at a dosage of 0.5 wt %, the intrinsic viscosity of the product is the highest, up to 1.05 ± 0.06 dL·g^{-1}. Therefore, the catalyst dosage in subsequent experiments is selected as 0.5 wt %.

Similarly, with the increase of the polymerization temperature, the intrinsic viscosity of the products is increased first and then decreased, and there is a maximum value of 1.08 ± 0.03 dL·g^{-1} at 170°C (Table 1, **Entries 2** and **11–15**). When the temperature is over 180°C, not only the intrinsic viscosity of the product is continuously decreased but also the color of the product is changed from white to light yellow. These

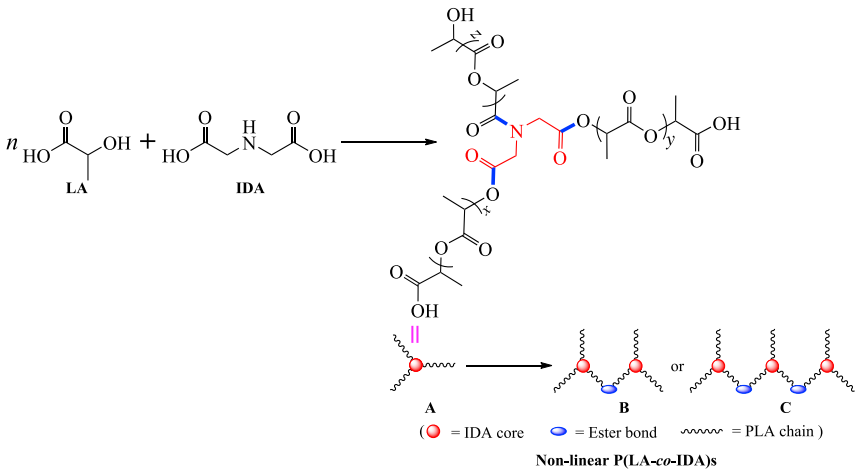

Scheme 3. Synthesis of non-linear P(LA-*co*-IDA)s

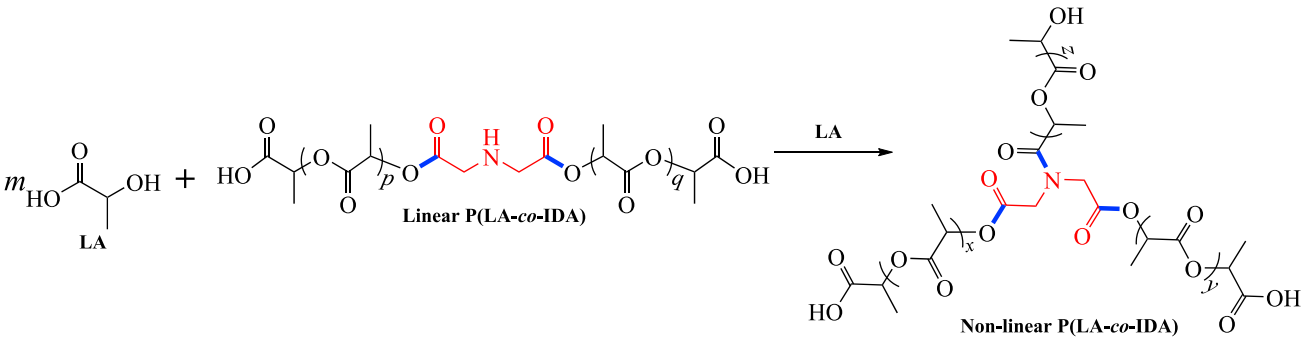

Scheme 4. P(LA-*co*-IDA) from linear to non-linear via amidation reaction

indicate that high temperature (190°C) may cause thermal degradation of the copolymer. As a result, the melting polymerization temperature in subsequent experiments is 170°C (**Entry 13**).

Finally, the polymerization time was investigated (Table 1, **Entries 13** and **16–19**). From 4 to 12 h, the intrinsic viscosity of the products is increased first and then decreased. There is a maximum value of 1.11 ± 0.02 $dL \cdot g^{-1}$ at 10 h, so the polymerization time is determined as 10 h (**Entry 18**).

In addition, we performed a multilinear regression analysis on the screening experiments that are using SnO as catalyst (**Entries 2** and **6–19**). Taking catalyst dosage, reaction temperature, and reaction time as independent variables, and [η] as dependent variable, the results are shown in Tables S3 and S4. It is known that the value of Durbin-Watson is close to 2, indicating that the independence of the samples is good, and the value of variance inflation factor is less than 5, showing that there is no multicollinearity of the samples. These can guarantee that the regression analysis results are valid. From the fact that the R^2 is 0.399 and the significance of reaction temperature is 0.032 (less than 0.05), we can know that these condition screening experiments have achieved certain effects (their shortcomings will be discussed in the limitations of the study).

Thus, under the above screened conditions of 0.5 wt % SnO catalyst, polycondensation temperature of 170°C, and reaction time of 10 h, serial P(LA-*co*-IDA) copolymers with different molar feed ratios, such as *n*(LA): *n*(IDA) = 8:1, 16:1, 32:1, 64:1, and 128:1, were directly synthesized via melt polycondensation, and the corresponding products were named as IDA8, IDA16, IDA32, IDA64, and IDA128, respectively.

Effects of different feeding ratios

The appearance, yield, and molecular weight of P(LA-*co*-IDA)s obtained from different feeding ratios are shown in Table 2. It can be seen that, with the increase of *n*(LA): *n*(IDA), the copolymers are all white powders, and all of them can be completely dissolved in $CHCl_3$, CH_3OH, and DMSO.

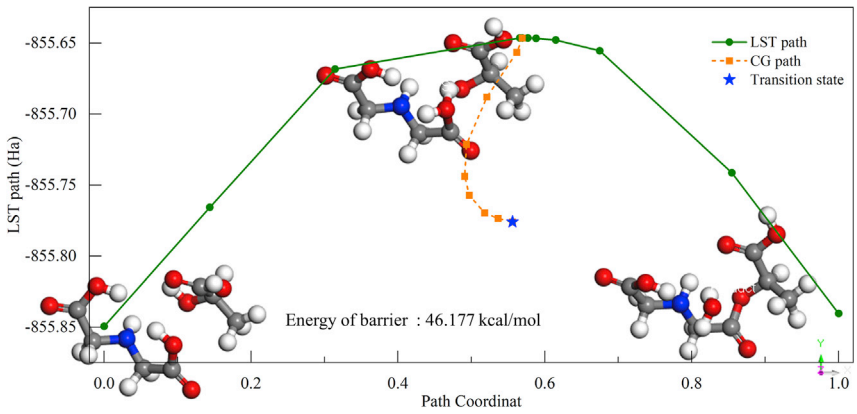

Figure 1. The transition state and energy barrier of the first esterification reaction between LA and IDA

Table 1. The effects of different factors on the appearance, yield, and intrinsic viscosity of copolymer

Entry	Catalyst type	Catalyst dosage (wt %)	Temperature (°C)	Time (h)	Appearance	Yield (%)	$[\eta]^a$ ($dL \cdot g^{-1}$)
1	Blank	0.5	160	8	Light gray powder	31	0.44 ± 0.05
2	**SnO**	**0.5**	**160**	**8**	**White powder**	**42**	**1.05** ± 0.06
3	ZnO	0.5	160	8	Gray powder	40	0.69 ± 0.05
4	$SnCl_2$	0.5	160	8	Light gray powder	44	0.83 ± 0.11
5	$ZnCl_2$	0.5	160	8	Light gray powder	59	0.42 ± 0.06
6	SnO	0.1	160	8	White powder	51	0.48 ± 0.03
7	SnO	0.3	160	8	White powder	60	0.71 ± 0.03
8	SnO	0.7	160	8	White powder	41	0.90 ± 0.02
9	SnO	0.9	160	8	White powder	48	0.54 ± 0.03
10	SnO	1.1	160	8	White powder	49	0.55 ± 0.03
11	SnO	0.5	140	8	White powder	60	0.55 ± 0.04
12	SnO	0.5	150	8	White powder	52	0.82 ± 0.02
13	**SnO**	**0.5**	**170**	**8**	**White powder**	**47**	**1.08** ± 0.03
14	SnO	0.5	180	8	White powder	46	1.02 ± 0.04
15	SnO	0.5	190	8	Yellowish powder	57	0.96 ± 0.06
16	SnO	0.5	170	4	White powder	58	0.87 ± 0.03
17	SnO	0.5	170	6	White powder	57	0.90 ± 0.03
18	**SnO**	**0.5**	**170**	**10**	**White powder**	**50**	**1.11** ± 0.02
19	SnO	0.5	170	12	White powder	53	1.04 ± 0.04

The entries in bold is the optimal condition in the every single-factor experiment.
[a]The freedom degree of uncertainty is 2.

For the yield of copolymers as the increase of *n*(LA): *n*(IDA), it is increased first and then decreased, possibly due to different reasons. When the *n*(LA): *n*(IDA) is small, there are more IDA active sites to produce more low-molecular-weight copolymers, which can be easily removed during the purification. However, once *n*(LA): *n*(IDA) is too large, LA is more likely to escape out of the reaction system under vacuum in the form of lactide, resulting in a decrease of the yield also.

The gel permeation chromatography (GPC) test results are shown in Figure 2, and the corresponding data are summarized in Table 2. It can be seen that, with the increase of *n*(LA): *n*(IDA), there is a gradual increase in the M_w and M_n of the products, while all the GPC curves are unimodal (Figure 2) and all the values of PDI are less than 2 (Table 2). These indicate that all products are the copolymers of LA and IDA indeed, rather than a mixture of copolymers and homopolymers, or multiple homopolymers (Xiong et al., 1991). Of course, the structure of copolymers is well characterized with Fourier transform infrared (FTIR) and ^{1}H NMR specctroscopies.

Structure characterization of copolymers

Some samples are used as representatives for the systematic analysis of the structure characterization by FTIR and ^{1}H NMR. The FTIR spectrum of IDA32 (Figure S4) and its peak assignments are shown in supplemental information. In contrast with the spectrum of homopolymer PLA synthesized via direct melt polycondensation (Zhao et al., 2005), there are not only peaks at 2,998, 2,947, and 1,758 cm^{-1} similar to PLA but also some characteristic absorption peaks, such as the peak at 3,643 cm^{-1} from unreacted NH in

Table 2. The effects of molar feed ratio on appearance, solubility, and yield

Samples	Appearance	Yield (%)	M_w (Da)	M_n (Da)	PDI
IDA8	White powder	52	4,800	3,200	1.50
IDA16	White powder	51	5,000	3,200	1.56
IDA32	White powder	62	6,500	4,100	1.58
IDA64	White powder	63	8,600	7,000	1.22
IDA128	White powder	53	11,400	7,800	1.46

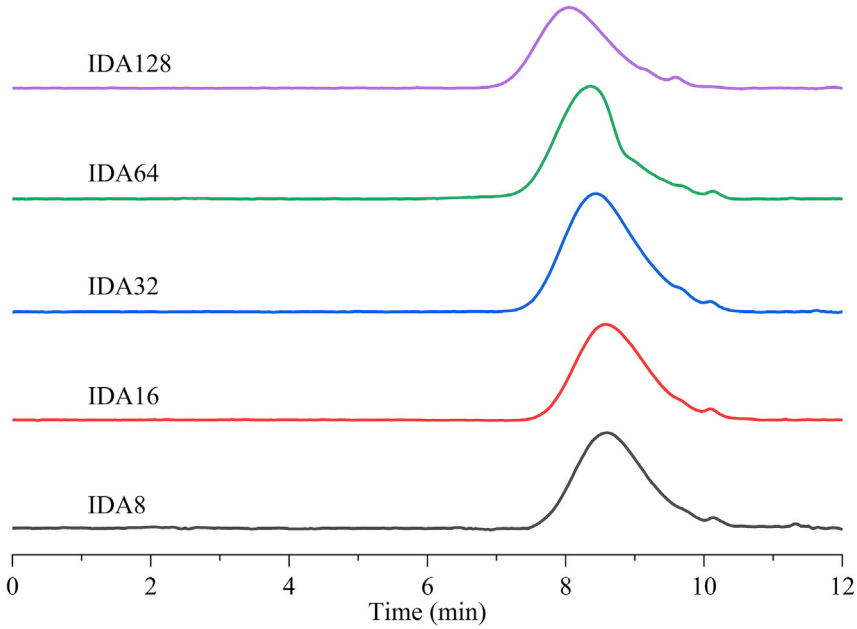

Figure 2. GPC curves of P(LA-*co*-IDA)s

IDA and the peak at 1,629 cm^{-1} from amide group, which are obviously not assigned to PLA. Therefore the product IDA32 obtained under the screened synthesis conditions are from the condensation of LA and IDA. Aldo, IDA32 contains both the linear and non-linear copolymers, which is consistent with the predicted structure of the chemical calculation results.

Moreover, according to the FTIR spectra of the P(LA-*co*-IDA)s synthesized by different molar feeding ratios (Figure 3), the peak positions and shapes of all curves are similar, and there are obvious variation rules showing the effects of feeding ratios. With the increase of *n*(LA): *n*(IDA), the peaks at 3,643 cm^{-1} from the unreacted NH in IDA, at 3,514 cm^{-1} from the terminal OH, and at 1,629 cm^{-1} from the C=O of amide group are all continuously weakened. These results reflect the impact of the reduction of IDA feeding amount, showing that IDA monomers can effectively participate in the copolymerization reaction under all different molar feeding ratios.

Using IDA32 as a representative (Figure 4), the ^{1}H NMR data are listed in the following (600 MHz, $CDCl_3$ as solvent, TMS as internal standard, δ, ppm): 1.45–1.50 ($H_{a'}$, C**H**$_3$ in the terminal LA unit), 1.53–1.60 (H_a, C**H**$_3$ in the LA segment), 2.95–3.03 ($H_{b'}$, C**H**$_2$ in the unamidated IDA units), 4.10–4.45 (H_b, C**H**$_2$ in the amidated IDA units, and $H_{c''}$, C**H** in the terminal LA unit of the amide bond-attached LA chain), 5.15–5.22 ($H_{c,c'}$, C**H** in the LA unit). These data show that IDA32 is mainly non-linear structure and contains a small amount of linear structure at the same time.

Furthermore, it can be seen from the ^{1}H NMR test results (Figure S5) of the P(LA-*co*-IDA)s obtained at different molar ratios that the chemical shift of all products are similar (Table S5). Combining with the results from FTIR spectra (Figure 3), it can be determined that all products are copolymers of IDA and LA. On the other hand, the ratio of the non-linear copolymer to the linear copolymer can be calculated from the integral area ratio of peak H_b and $H_{b'}$, and the average value of all samples is 11.39:1 (Table S6). Similarly, the content of the non-linear structure can be calculated, and the average value of all samples is 92% (Table S6). These results once again show that the products are dominated by non-linear structure, which is consistent with the structure predicted by Scheme 3.

Moreover, the molecular weight M_n of P(LA-*co*-IDA) was calculated based on the ^{1}H NMR data according to the reported method (Lin et al., 2020; Luo et al., 2011, 2019); the obtained results are shown in Table S7. We can know that, with the increase of *n*(LA): *n*(IDA), the M_n generally shows an increasing trend, which is consistent with the trend of M_n tested by GPC. Meanwhile, for IDA8, IDA16, and IDA32, the two M_n are relatively similar. However, for IDA64 and IDA128, they are quite different. Thus, it is possible that both IDA64

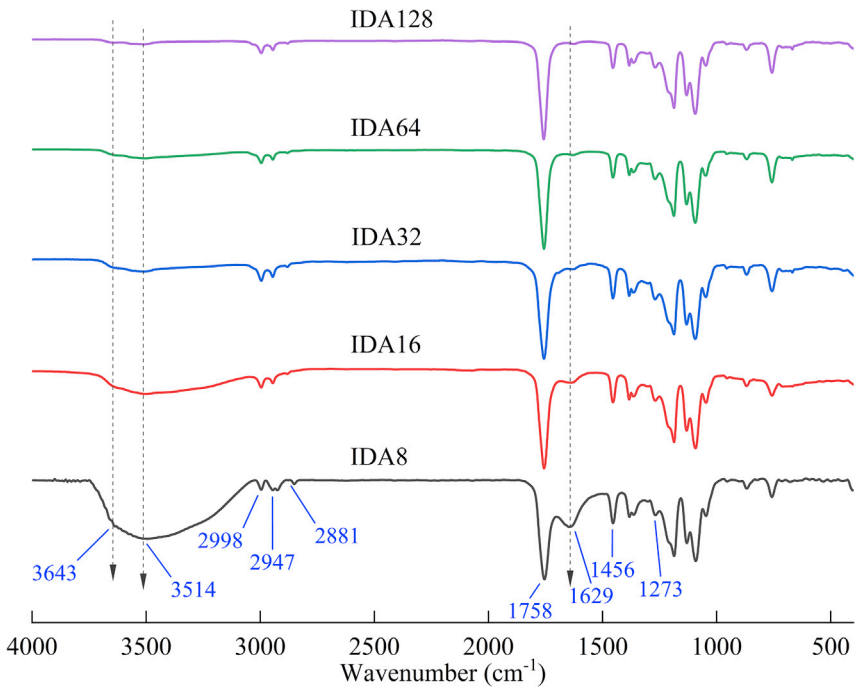

Figure 3. FTIR spectra of P(LA-*co*-IDA)s

and IDA128 are not simple one-core structure copolymers, because their more repeating LA units and longer chains on each arm allow a greater spatial activity, resulting in a smaller relative steric hindrance to form multi-core molecules.

In order to prove this prediction, the M_n of IDA64 and IDA128 as multi-core model (Table S7) were further calculated by the data of ^{1}H NMR referring to the reported method (Wang et al., 2011; Luo et al., 2011). It can be seen that, in the two-core model, their M_n is closer to the M_n tested by GPC, but still obviously less than the latter. In the three-core model, their M_n is closer to the M_n tested by GPC, but slightly higher than the latter. So, there are both two-core and three-core copolymers in IDA64 and IDA128.

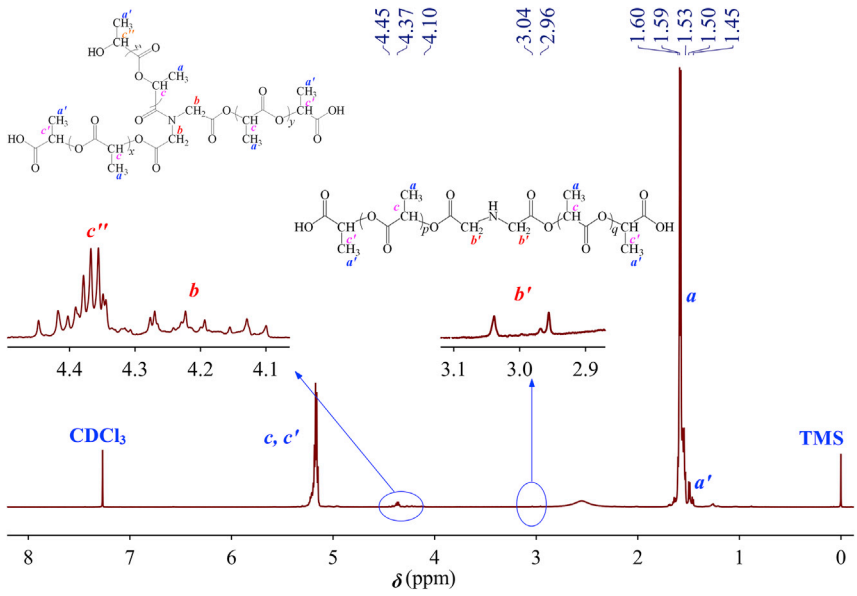

Figure 4. ^{1}H NMR spectrum of IDA32

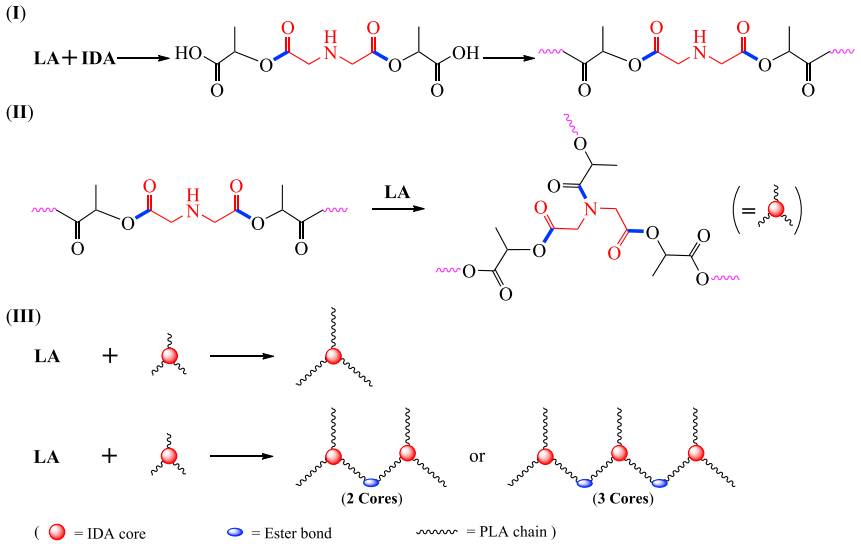

Scheme 5. Schematic diagram of the possible reaction mechanism

On the basis of the aforementioned results, it can be inferred that the process of the polymer formation should be diverse under different *n*(LA): *n*(IDA), and the polymerization mechanism of the IDA-modified PLA may be briefly summarized as follows (Scheme 5):

(I) At the initial stage of the reaction, no matter what the molar feed ratio is, the first step of polymerization is the reaction between -OH on LA and -COOH on IDA to form ester bonds, mainly because the energy barrier of forming ester bonds is lower than that of forming amide bonds. Then, the LA chains at both ends of IDA begin to grow continuously to form linear molecules. Conversely, if the first step is the reaction between -COOH on LA and -NH on IDA to form amide bonds, there will be no unreacted -NH groups due to the high stability of amide bond. This is not only in conflict with the results of chemical calculations but also inconsistent with the test results of FTIR and ^{1}H NMR.

(II) The second step is the continuous growth of linear molecules, as well as the formation of amide bonds by the reaction of -COOH on LA and -NH on IDA, and then the growth of LA chain on the new arm connecting with the IDA core with amide bond. After the simultaneous growth of these chains, a star-shaped copolymer with three arms can be produced.

(III) With the formation of three-arm copolymer, IDA8, IDA16, and IDA32 are obtained under a small ratio of *n*(LA): *n*(IDA) and are difficult to further form multi-core copolymer, due to the inflexible segment motion of short PLA chains. However, under a large ratio of *n*(LA): *n*(IDA), the PLA chain are long enough to produce a flexible segment motion, leading to an easier formation of multi-core structure. As a result, the products, such as IDA64 and IDA128, mainly having two-core and three-core structure, can be obtained.

Physical properties of copolymers

The X-ray diffraction (XRD) test results of P(LA-*co*-IDA)s (Figure S6 and Table S8) show that all copolymers have high crystallinity and their diffraction peak positions are similar to that of PLA prepared by direct melt polymerization (Zhao et al., 2005). With the increase of *n*(LA): *n*(IDA), the crystallinity of the copolymers shows a downward trend. Perhaps, for IDA8, IDA16, and IDA32, the *n*(LA): *n*(IDA) is relatively smaller, there is a higher content for IDA unit, and there is a stronger hydrogen bond between molecules. Especially, a shorter PLA arm and a lower M_n of the star-shaped copolymer with one-core makes the whole macromolecule tend to stretch into a three-arm plane, more easily leading to a regular arrangement formation. In contrast, the crystallinity of IDA64 and IDA128 is significantly lower, because the above-mentioned characteristics are just the opposite of the copolymers obtained at the smaller ratio of *n*(LA): *n*(IDA); these make the whole macromolecule with two- or three-core structure difficult to stretch into a similar plane and there is a more irregular molecular arrangement.

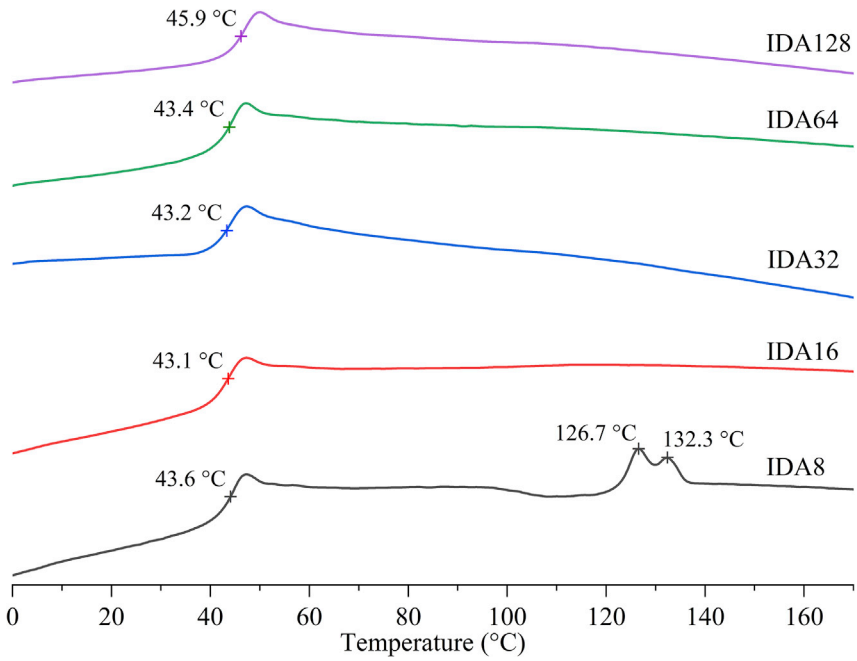

Figure 5. DSC curves of P(LA-*co*-IDA)s

The DSC second heating curves of P(LA-*co*-IDA)s are shown as Figure 5, and the data are summarized in Table S9. We can know that, there is only one glass transition process on all DSC curves. This further indicates that the products prepared by direct melt polycondensation of LA and IDA should be copolymers indeed, rather than physical blends of multiple homopolymers (Xiong et al., 1991). With the exception of IDA8, no endothermic peak appears on the DSC curves of all other samples. This indicates that there is the stronger hydrogen bond force between IDA8 molecules indeed as mentioned above, making them easier to produce recrystallization during the first cooling process. And in the recrystallization process, different types of crystal, or complete and defective crystal grains in a same crystal type, may be generated at the same time (Makrani et al., 2019). Therefore, there are two melting peaks on the DCS curve of IDA8 (Table S9).

The thermogravimetric analysis (TG) test results are shown in Figure 6, and the data are summarized in Table S10. Obviously, for all copolymers, not only there is only one step on the TG curves but also there is only one peak on the derivative thermogravimetry curves (Figure S7). Thus, in the decomposition process, there is only one stage on the whole, which is mainly derived from the PLA chain decomposition (Wang et al., 2010). At the same time, with the increase of *n*(LA): *n*(IDA), the thermal decomposition onset temperature (T_o), maximum weight loss temperature (T_{max}), and termination temperature (T_t) of P(LA-*co*-IDA)s all show a decreasing trend, although the total weight loss rates of all samples are the same (Table S10). Among them, the T_o, T_{max}, and T_t of IDA8 and IDA16 are significantly higher than those of other samples. These indicate that the IDA unit in the P(LA-*co*-IDA)s improves the thermal stability of the modified PLA, because the content of nitrogen element incorporated into these copolymers is relatively higher (Xiong et al., 2014).

Degradation properties of copolymers

As per the reported method, (Wan et al., 2019a, 2019b), the degradation properties of P(LA-*co*-IDA)s were determined by gravimetric method in a pH-neutral deionized water solution at 37°C. The results are shown in Table 3. It can be found that there are three obvious characteristics as follows.

First, the degradation rates of IDA8, IDA16, and IDA32 are close to each other, whereas that of IDA64 is higher, and that of IDA128 is the highest (Figure S8). In combination with the XRD test results in Figure S6 and Table S8, the reason is speculated. Perhaps, the crystallinity and actual *n*(IDA): *n*(LA) of IDA8, IDA16, and IDA32 are relatively close to each other, whereas those of IDA64 are lower, and these of IDA128 are obviously the lowest. In general, the degradation of biodegradable polymers slows down as the crystallinity increases, because the amorphous phase is degraded faster than the crystalline phase (Zheng and Pan,

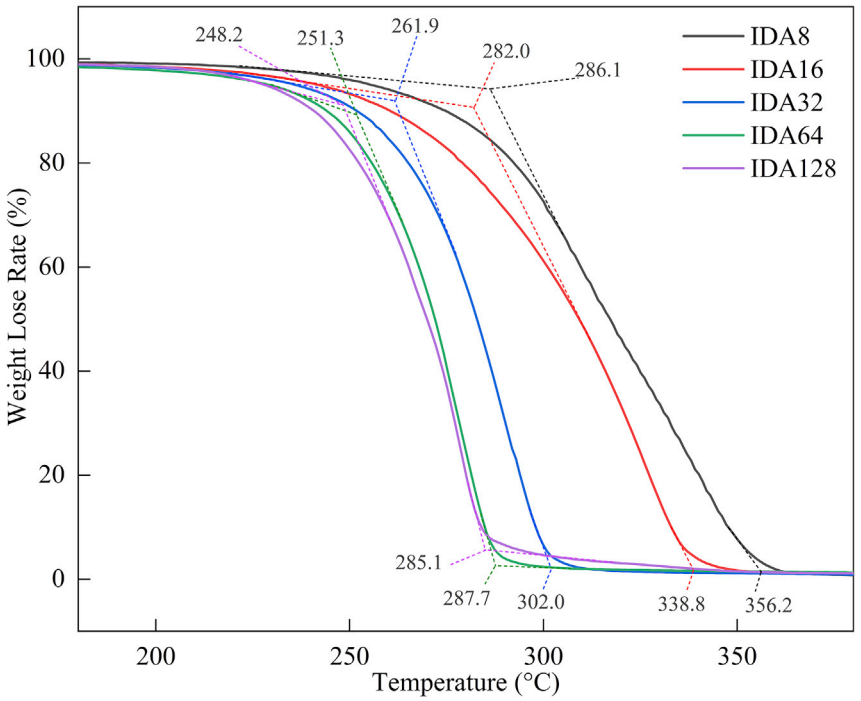

Figure 6. TG curves of P(LA-*co*-IDA)s

2020). This difference shows that the crystallinity and actual *n*(IDA): *n*(LA) of P(LA-*co*-IDA)s have a great influence on the degradation performance of the copolymers.

Second, for a copolymer obtained by the same molar feeding ratio, with the increase of the degradation time, its weekly degradation rate shows an increasing trend (Table 3). Importantly, comparing with the ring increase of degradation rate in last week, there is a self-accelerating effect. The possible reason is that the concentration of LA and H^+ in the degradation system is increased continuously, and H^+ can catalyze the acceleration of P(LA-*co*-IDA) degradation (Porfyris et al., 2018; Rocca-Smith et al., 2017).

Third, with the increase of *n*(LA): *n*(IDA), the ring increase of degradation rate shows a decrease trend (Table 3). The reasons may be that when the *n*(LA): *n*(IDA) is small (for IDA8, IDA16, and IDA32), the degradation of the copolymers is not obvious in the early stage; only as the degradation time increases, the H^+ concentration in the system is increased significantly, then the degradation of the copolymer in the later stage is accelerated. However, when the *n*(LA): *n*(IDA) is large (for IDA64 and IDA128), the copolymers are degraded obviously in the early stage, so there is little increase in the H^+ concentration with the increase of the degradation time, resulting in a smaller ring increase of degradation rate.

Lead ion chelating property of copolymers

The lead ion chelating property of copolymers was quantified by the method reported previously (Sedghi et al., 2015, 2017; Maratta et al., 2016). The detailed operation procedure is shown in the "STAR methods" section and Flow chart S1. The absorption curves and values of Pb^{2+} standard solutions in different concentrations are obtained, as shown in Figure S9. On the basis of Figure S9, a standard curve of concentration-absorption value relationship is drawn as Figure S10. Then, the relation equation (Equation 1) between Pb^{2+} concentration x' and UV-vis absorption value y' can be obtained by the linear fitting of the standard curve.

$$y' = 0.1328x' + 0.1042 \quad \text{(Equation 1)}$$

Similarly, the absorption curves and values of Pb^{2+} working solutions with an original concentration of 2 $mg \cdot L^{-1}$ at different degradation-chelation times are obtained, as shown in Figure S11. And then, by Equation 1, the final concentration of unchelated Pb^{2+} in the working solution can be calculated. Furthermore, the proportion of chelated Pb^{2+} in the working solution, namely, Pb^{2+} chelated rate [$R_{(Pb\ chelated)}$], can

Table 3. Degradation rate and its ring increase of P(LA-*co*-IDA)s at different time

	Degradation rate (%)				Ring increase of degradation rate (%)		
Samples	1 w	2 w	3 w	4 w	1→2 w	2→3 w	3→4 w
IDA8	11	15	22	40	36	47	82
IDA16	11	14	22	36	27	57	64
IDA32	12	18	27	41	50	50	52
IDA64	27	35	46	61	30	31	33
IDA128	36	44	55	70	22	25	27

be obtained from Equation 2 (the results are shown in Figure 7). In Equation 2, 2 is the original concentration of Pb^{2+} in the working solution and x' is the final concentration of unchelated Pb^{2+} in the working solution, the unit of both being $mg \cdot L^{-1}$.

$$R_{(Pb\ chelated)} = (2\text{-}x') / 2 \times 100\% \quad \text{(Equation 2)}$$

For the Pb^{2+} chelating performance of P(LA-*co*-IDA)s, it can be seen from Figure 7 that, in the first week, the Pb^{2+} chelating adsorption rates of all samples are basically similar. In the second week, the data of IDA16, IDA32, IDA64, and IDA128 are relatively similar, whereas the value of IDA8 is obviously higher. It is worth noting that in the third and fourth weeks, for all samples, there is a decreasing trend with the increase of *n*(LA): *n*(IDA). Perhaps, the reasons are that when the mass of the samples is the same, with the increase of *n*(LA): *n*(IDA), the M_n of P(LA-*co*-IDA) increases (Table 2), so that the number of molecules is decreased. At the same time, the proportion of IDA unit in the P(LA-*co*-IDA) molecule is also decreasing. Thus, the amount of IDA unit released from the samples is reduced, resulting in a decrease of Pb^{2+} chelating adsorption rate.

Importantly, the IDA released rate [$R_{(IDA\ released)}$] of P(LA-*co*-IDA) at the corresponding time can be calculated from the Pb^{2+} chelating adsorption rate. The calculation method is shown as Equation 3, and the results are summarized in Figure 8.

$$R_{(IDA\ released)} = M_{(IDA\ released)} / M_{(IDA\ total)} \quad \text{(Equation 3A)}$$

where $M_{(IDA\ released)}$ is the amount of substance of IDA released by the P(LA-*co*-IDA) degradation. As IDA and Pb^{2+} are chelated in the ratio 1:1, $M_{(IDA\ released)}$ is equal to $M_{(Pb\ chelated)}$ and $M_{(Pb\ chelated)}$ is the amount of Pb^{2+} chelated in the reaction flask and can be calculated by Equation 3B.

$$M_{(IDA\ released)} = M_{(Pb\ chelated)} = R_{(Pb\ chelated)} \times 0.1 \times 2 / (207 \times 1000) \quad \text{(Equation 3B)}$$

In Equation 3B, 0.1 is the volume of the Pb^{2+} working solution in reaction flask, the unit is L; 2 is the original Pb^{2+} concentration of the working solution, the unit is $mg \cdot L^{-1}$; 207 is the molecular weight of Pb^{2+}, the unit is $g \cdot mol^{-1}$; and 1,000 is the conversion factor of mg and g.

$M_{(IDA\ total)}$ is the total amount of substance of IDA contained in the P(LA-*co*-IDA) sample, which can be calculated by Equation 3C.

$$M_{(IDA\ total)} = 250 / (M_n \times r \times 1000) \quad \text{(Equation 3C)}$$

In Equation 3C, 250 is the mass of the P(LA-*co*-IDA) sample added into the reaction flask, the unit is mg; M_n is the molecular weight of P(LA-*co*-IDA) measured by GPC as shown in Table 2, the unit is $g \cdot mol^{-1}$; r is the actual *n*(LA): *n*(IDA) of P(LA-*co*-IDA) measured by ^1H NMR as shown in Table S5; and 1,000 is the conversion coefficient between mg and g.

From Figure 8, we can know that $R_{(IDA\ released)}$ is increased with the increase of *n*(LA): *n*(IDA) during the process of sample degradation and IDA release. The reasons may be that with the increase of *n*(LA): *n*(IDA), the proportion of LA in the copolymer molecule is increased and the proportion of IDA is decreased, so the self-catalytic degradation effect produced by H^+ is enhanced, whereas the intermolecular hydrogen bond force is weakened. Both are beneficial to promote the degradation and IDA release of samples.

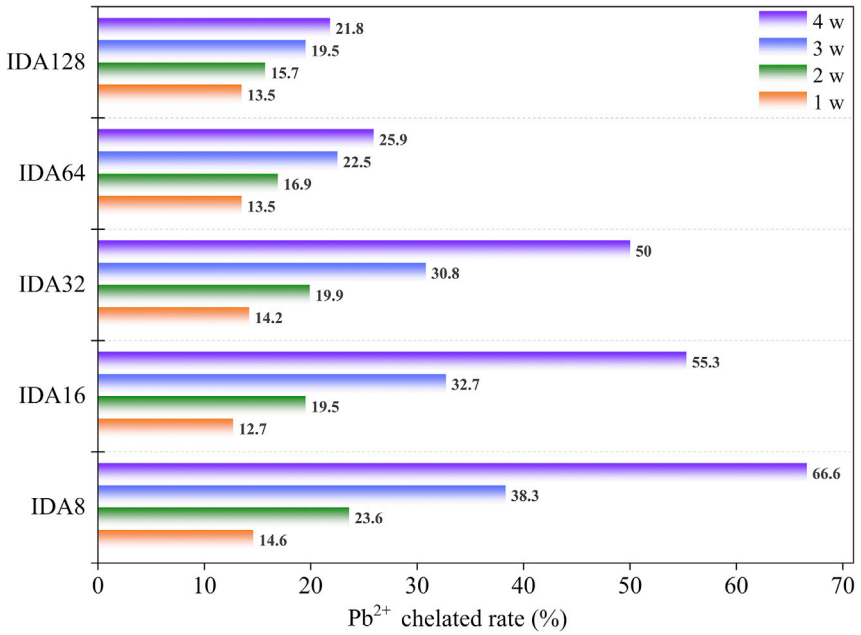

Figure 7. Pb^{2+} chelated rates of P(LA-*co*-IDA)s at different time

Interestingly, it can also be seen from Figure 8 that the change trend of $R_{(IDA\ released)}$ calculated from the UV-vis method data, is generally consistent with the degradation rate calculated from the gravimetric method data. The reason is simple in fact, because the release of IDA originates from the degradation of P(LA-*co*-IDA). However, there is also a certain gap between the two curves, and the degradation rate of most samples is higher than their $R_{(IDA\ released)}$ for most samples. The difference may be because when some incompletely degraded samples are dissolved and suspended in water, they are removed in the solid-liquid separation.

Even so, according to the same trends and the reasonable gaps between degradation rate and $R_{(IDA\ released)}$, especially the data of the products from small feeding ratios in the first three weeks and those of the products from all feeding ratios in the fourth week, for PLA materials modified by the comonomers without any fluorescent groups, although these comonomers cannot be detected by UV-vis absorption method to monitor their release rate, they may be indirectly monitored by the gravimetric method.

At last, the Pb^{2+} chelating capacity (C) of P(LA-*co*-IDA)s can be calculated from its IDA release rate and Pb^{2+} chelating rate at a certain time point, as shown in Equation 4. In the formula, 2 is the concentration of the test solution, the unit is $mg \cdot L^{-1}$; 0.1 is the volume of the test solution, the unit is L; 1,000 is the conversion coefficient between g and mg; and 250 is the mass of the sample in the test bottle, the unit is mg.

$$C = [2 \times 0.1 \times R_{(Pb\ chelated)}] \times [1 / R_{(IDA\ released)}] \times [1000 / 250] \quad \text{(Equation 4)}$$

Herein, the chelating capacity of P(LA-*co*-IDA)s was calculated on the basis of the IDA release rate and Pb^{2+} chelation rate in the fourth week. From the results shown in Figure S12, we come to know that with the increase of *n*(LA): *n*(IDA), the Pb^{2+} chelating capacity of P(LA-*co*-IDA)s is gradually decreased from 1.80 $mg \cdot g^{-1}$ of IDA8 to 0.33 $mg \cdot g^{-1}$ of IDA128. The datum is similar to (Tahtat et al., 2017; El-Ashgar et al., 2017) or higher than (Liu et al., 2020; Blicharska et al., 2018) that of the reported polymeric (or M_w over 1,200 Da) Pb^{2+} chelators using IDA or other substances as functional groups. Importantly, this level of chelating capacity is suitable for a potential biomedical chelating agent as a treatment drug for chelating and removing lead ions *in vivo* because the threshold of lead poisoning that requires treatment is 10 $\mu g \cdot dL^{-1}$ (Balasubramanian et al., 2020), and the corresponding dosage of small molecule chelating drugs is as low as 30 $mg \cdot kg^{-1}$ body weight per day (Safi et al., 2019). This can avoid toxicity and adverse reactions caused by a high dosage of the chelating drugs (Hsiao et al., 2019; Bradberry and Vale, 2009).

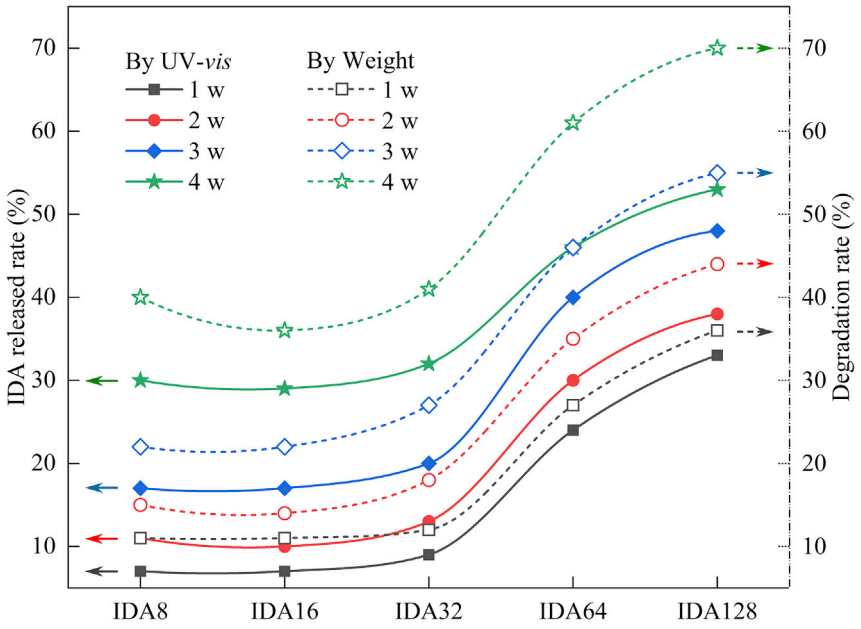

Figure 8. IDA release rate at different time of P(LA-*co*-IDA)s

In addition, the result also indicates that this Pb^{2+} chelating capacity can be adjusted according to the need of the practical application.

In a word, by adjusting the molar feeding ratio *n*(LA): *n*(IDA), it can be found that with the increase of *n*(LA): *n*(IDA), the Pb^{2+} chelating capacity of the copolymers is decreased gradually. In contrast, for their degradation rate and IDA release rate, there is a gradual increase trend almost synchronously. Thus, according to these regular changes, it is expected to develop a test method for the sustained release of functional monomer without fluorescent groups from PLA materials.

Conclusions

For the first time, the bio-based LA is used to copolymerize with the common metal ion chelating agent IDA. Under the screened synthetic conditions, a series of novel polymeric sustained-release Pb^{2+} chelating agent P(LA-*co*-IDA)s are obtained by one-step reaction. The theoretical calculation and structural characterization with FTIR, ^{1}H NMR, and GPC show P(LA-*co*-IDA)s mainly having star-shaped structure, and some star-shaped copolymers with two-core or three-core structures can be found, especially for IDA64 and IDA128. With the change of molar feed ratio, the performance and properties of P(LA-*co*-IDA)s generally show regular variation. Importantly, P(LA-*co*-IDA)s have been proved to have Pb^{2+} chelating function as designed. With the increase of *n*(LA): *n*(IDA), Pb^{2+} chelating capability of P(LA-*co*-IDA) is decreased, but its IDA release rate is increased gradually. At the same time, the change of the degradation rate measured by gravimetric method is consistent with the altering trend of the IDA release rate measured by UV-vis method. Thus, not only P(LA-*co*-IDA) is expected to be developed as lead poisoning treatment drugs or Pb^{2+} adsorbents in the environment with long-lasting effect but also a similar method to measure the sustained release rate of functional monomer without any fluorophore groups from PLA materials can be developed.

Limitations of the study

The one-variable-at-a-time method, which is commonly used in the field of organic chemistry, was used to screen the reaction conditions in this work, and was verified by multiple linear regression analysis. It is found that, for the main dependent variable [η], the independent variable of reaction temperature has a significant influence on it, whereas the independent variables such as the amount of catalyst and reaction time have no significant influence on it. In subsequent studies, design of experiment method should be used to optimize the reaction conditions.

STAR★METHODS

Detailed methods are provided in the online version of this paper and include the following:

- KEY RESOURCES TABLE
- RESOURCE AVAILABILITY
  - Lead contact
  - Materials availability
  - Data and code availability
- METHOD DETAILS
  - Materials
  - Theoretical computation
  - Synthesis of copolymers
  - Structure characterization
  - Tests of physical properties
  - Degradation test
  - Lead ion chelating test
- QUANTIFICATION AND STATISTICAL ANALYSIS
- ADDITIONAL RESOURCES

SUPPLEMENTAL INFORMATION

Supplemental information can be found online at https://doi.org/10.1016/j.isci.2021.102518.

ACKNOWLEDGMENTS

This research was supported by the Open Fund of the Key Laboratory of Functional Molecular Engineering of Guangdong Province in SCUT (No. 2017kf01), the National Natural Science Foundation of China (20772035), and the Guangdong Basic and Applied Basic Research Foundation (No. 2021A1515012342).

AUTHOR CONTRIBUTIONS

Conceptualization, J.-Y.L.; investigation, J.-Y.L. and J.-X.W.; writing – original draft, J.-Y.L.; writing – review & editing, J.-Y.L., Z.W., X.-Y.C., Y.X., and Y.-G.F.; funding acquisition, Z.-Y.W. and S.-H.L.; supervision, L.-T.Y.; project administration, Z.-Y.W.

DECLARATION OF INTERESTS

The authors declare no competing interests.

Received: January 12, 2021
Revised: April 4, 2021
Accepted: May 4, 2021
Published: June 25, 2021

REFERENCES

Amphlett, J.T.M., Sharrad, C.A., and Ogden, M.D. (2018). Extraction of uranium from non-saline and hypersaline conditions using iminodiacetic acid chelating resin Purolite S930+. Chem. Eng. J. *342*, 133–141.

An, F.-Q., Wu, R.-Y., Li, M., Hu, T.-P., Gao, J.-F., and Yuan, Z.-G. (2017). Adsorption of heavy metal ions by iminodiacetic acid functionalized D301 resin: kinetics, isotherms and thermodynamics. React. Funct. Polym. *118*, 42–50.

Anito, D.A., Wang, T.X., Liu, Z.W., Ding, X.S., and Han, B.H. (2020). Iminodiacetic acid-functionalized porous polymer for removal of toxic metal ions from water. J. Hazard. Mater. *400*, 123188.

Ayers, P.W., and Parr, R.G. (2000). Variational principles for describing chemical reactions: the Fukui function and chemical hardness revisited. J. Am. Chem. Soc. *122*, 8731–8744.

Balasubramanian, B., Meyyazhagan, A., Chinnappan, A.J., Alagamuthu, K.K., Shanmugam, S., Al-Dhabi, N.A., Ghilan, A.K.M., Duraipandiyan, V., and Arasu, M.V. (2020). Occupational health hazards on workers exposure to lead (Pb): a genotoxicity analysis. J. Infect. Public Health *13*, 527–531.

Blicharska, E., Tatarczak-Michalewska, M., Plazinska, A., Plazinski, W., Kowalska, A., Madejska, A., Szymanska-Chargot, M., Sroka-Bartnicka, A., and Flieger, J. (2018). Solid-phase extraction using octadecyl-bonded silica modified with photosynthetic pigments from Spinacia oleracea L. for the preconcentration of lead(II) ions from aqueous samples. J. Sep. Sci. *41*, 3129–3142.

Bradberry, S., and Vale, A. (2009). Dimercaptosuccinic acid (succimer; DMSA) in inorganic lead poisoning. Clin. Toxicol. *47*, 617–631.

Bretti, C., Cigala, R.M., De Stefano, C., Lando, G., and Sammartano, S. (2017). Understanding the bioavailability and sequestration of different metal cations in the presence of a biodegradable chelant MGDA in biological fluids and natural waters. Chemosphere *183*, 107–118.

Bretti, C., Cigala, R.M., De Stefano, C., Lando, G., and Sammartano, S. (2019). Thermodynamic study on polyaspartic acid biopolymer in solution

and prediction of its chemical speciation and bioavailability in natural fluids. J. Mol. Liq. *274*, 68–76.

Byun, J., and Han, J. (2020). Sustainable development of biorefineries: Integrated assessment method for co-production pathways. Energ. Environ. Sci. *13*, 2233–2242.

Calvino, C., Macke, N., Kato, R., and Rowan, S.J. (2020). Development, processing and applications of bio-sourced cellulose nanocrystal composites. Prog. Polym. Sci. *103*, 101221.

Charton, J., Gauriot, M., Guo, Q., Hennuyer, N., Marechal, X., Dumont, J., Hamdane, M., Pottiez, V., Landry, V., Sperandio, O., et al. (2014). Imidazole-derived 2-[N-carbamoylmethylalkyl-amino]acetic acids, substrate-dependent modulators of insulin-degrading enzyme in amyloid- *β* hydrolysis. Eur. J. Med. Chem. *79*, 184–193.

Charton, J., Gauriot, M., Totobenazara, J., Hennuyer, N., Dumont, J., Bosc, D., Marechal, X., Elbakali, J., Herledan, A., Wen, X.A., et al. (2015). Structure-activity relationships of imidazole-derived 2-[*N*-carbamoylmethyl- alkylamino] acetic acids, dual binders of human insulin-degrading enzyme. Eur. J. Med. Chem. *90*, 547–567.

Chen, T.T.D., Carrodeguas, L.P., Sulley, G.S., Gregory, G.L., and Williams, C.K. (2020). Bio-based and degradable block polyester pressure-sensitive adhesives. Angew. Chem. Int. Ed. *59*, 23450–23455.

El-Ashgar, N.M., Silmi, M.K., El-Nahhal, I.M., Chehimi, M.M., and Babonneau, F. (2017). Template synthesis of iminodiacetic acid polysiloxane immobilized ligand systems and their metal uptake capacity. Silicon *9*, 563–575.

Faveere, W., Van Praet, S., Vermeeren, B., Dumoleijn, K.N.R., Moonen, K., Taarning, E., and Sels, B.F. (2020). Toward replacing ethylene oxide in a sustainable world: Glycolaldehyde as bio-based C2 platform molecule. Angew. Chem. Int. Ed. *34*, 67–76.

Fruk, L., Franck, C.O., Fanslau, L., Andrea Bistrovic, P., and Tyagi, P. (2021). Biopolymer-based carriers for DNA vaccine design. Angew. Chem. Int. Ed. https://doi.org/10.1002/anie.202010282.

Fry, K.L., Wheeler, C.A., Gillings, M.M., Flegal, A.R., and Taylor, M.P. (2020). Anthropogenic contamination of residential environments from smelter As, Cu and Pb emissions: Implications for human health. Environ. Pollut. *262*, 114235.

Giraud, L., Grelier, S., Grau, E., Hadziioannou, G., Brochon, C., Cramail, H., and Cloutet, E. (2020). Upgrading the chemistry of pi-conjugated polymers toward more sustainable materials. J. Mater. Chem. C *8*, 9792–9810.

Gokcal, B., Kip, C., Sahinbas, D., Celik, E., and Tuncel, A. (2020). Silica microspheres functionalized with the iminodiacetic acid/copper(II) complex as a peroxidase mimic for use in metal affinity chromatography-based colorimetric determination of histidine-tagged proteins. Microchim. Acta *187*, 121.

Gorantla, K.R., and Mallik, B.S. (2020). Iron complex as a water-oxidizing catalyst: free-energy barriers, proton-coupled electron transfer, spin dynamics, and role of water molecules in the reaction mechanism. J. Phys. Chem. C *124*, 205–218.

He, X.M., Zhang, J., Ren, Y.N., Sun, C.Y., Deng, X.P., Qian, M., Hu, Z.B., Li, R., Chen, Y.H., Shen, Z.G., and Xia, Y. (2019a). Polyaspartate and liquid amino acid fertilizer are appropriate alternatives for promoting the phytoextraction of cadmium and lead in Solanum nigrum L. Chemosphere *237*, 124483.

He, Y.X., Eloi, J.C., Harniman, R.L., Richardson, R.M., Whittell, G.R., Mathers, R.T., Dove, A.P., O'Reilly, R.K., and Manners, I. (2019b). Uniform biodegradable fiber-like micelles and block comicelles *via* "Living" crystallization-driven self-assembly of poly(L-lactide) block copolymers: the importance of reducing unimer self-nucleation *via* hydrogen bond disruption. J. Am. Chem. Soc. *141*, 19088–19098.

Hermann, A., Hill, S., Metz, A., Heck, J., Hoffmann, A., Hartmann, L., and Herres-Pawlis, S. (2020). Next generation of zinc bisguanidine polymerization catalysts towards highly crystalline, biodegradable polyesters. Angew. Chem. Int. Ed. *59*, 21778–21784.

Hsiao, C.Y., Gresham, C., and Marshall, M.R. (2019). Treatment of lead and arsenic poisoning in anuric patients - a case report and narrative review of the literature. BMC Nephrol. *20*, 374.

Hu, X., Lee, W.H., Zhao, J.Y., Bae, J.Y., Kim, J.S., Wang, Z., Yan, J.L., Zhuang, Y.B., and Lee, Y.M. (2020). Troger's Base (TB) - containing polyimide membranes derived from bio-based dianhydrides for gas separations. J. Membr. Sci. *610*, 118255.

Leydier, A., Lin, Y., Arrachart, G., Turgis, R., Lecercle, D., Favre-Reguillon, A., Taran, F., Lemaire, M., and Pellet-Rostaing, S. (2012). EDTA and DTPA modified ligands as sequestering agents for uranyl decorporation. Tetrahedron *68*, 1163–1170.

Liao, Y.H., Koelewijn, S.F., Van den Bossche, G., Van Aelst, J., Van den Bosch, S., Renders, T., Navare, K., Nicolai, T., Van Aelst, K., Maesen, M., et al. (2020). A sustainable wood biorefinery for low-carbon footprint chemicals production. Science *367*, 1385–1390.

Lin, J.-Y., Luo, S.-H., Yang, C.-L., Xiao, Y., Yang, L.-T., and Wang, Z.-Y. (2021). Bio-based polymeric hemostatic material and wound dressing. Prog. Chem. https://doi.org/10.7536/PC 200437.

Lin, J.-Y., Luo, S.-H., Chen, S.-H., Yang, L.-T., Xiao, Y., Huang, Z.-H., and Wang, Z.-Y. (2020). Efficient synthesis, characterization, and application of biobased scab-bionic hemostatic polymers. Polym. J. *52*, 615–627.

Lin, Z.S., Zhang, Y.R., Ober, C.K., and Goddard, J.M. (2018). Facile preparation of epoxide-functionalized surfaces *via* photocurable copolymer coatings and subsequent immobilization of iminodiacetic acids. ACS Appl. Mater. Interfaces *10*, 40871–40879.

Liu, Z.Y., Xu, T.T., Wang, M., Mao, C., and Chi, B. (2020). Magnetic mesoporous silica/epsilon-polylysine nanomotor-based removers of blood Pb^{2+}. J. Mater. Chem. B *8*, 11055–11062.

Lu, T., and Manzetti, S. (2014). Wavefunction and reactivity study of benzo[a]pyrene diol epoxide and its enantiomeric forms. Struct. Chem. *25*, 1521–1533.

Luo, S.-H., Wang, Z.-Y., Mao, C.-X., and Huo, J.-P. (2011). Synthesis of biodegradable material poly(lactic acid-*co*-glycerol) *via* direct melt polycondensation and its reaction mechanism. J. Polym. Res. *18*, 2093–2102.

Luo, S.-H., Wu, Y.-C., Cao, L., Lin, J.-Y., Gao, J., Chen, S.-X., and Wang, Z.-Y. (2019). Direct metal-free preparation of functionalizable polylactic acid-ethisterone conjugates in a one-pot approach. Macromol. Chem. Phys. *220*, 1800475.

Luo, S.-H., Wu, Y.-C., Cao, L., Wang, Q.-F., Chen, S.-X., Hao, Z.-F., Jing, L., and Wang, Z.-Y. (2017). One-pot preparation of polylactic acid-ibuprofen conjugates and their performance characterization. Polym. Chem. *8*, 7009–7016.

Maiti, S., Karan, S.K., Kim, J.K., and Khatua, B.B. (2019). Nature driven bio-piezoelectric/triboelectric nanogenerator as next-generation green energy harvester for smart and pollution free society. Adv. Energy Mater. *9*, 1803027.

Makrani, N., Ammari, A., Benrekaa, N., Rodrigue, D., and Giroux, Y. (2019). Dynamics of the *α*-relaxation during the crystallization of PLLA and the effect of thermal annealing under humid atmosphere. Polym. Degrad. Stab. *164*, 90–101.

Maratta, A., Vazquez, S., Lopez, A., Augusto, M., and Pacheco, P.H. (2016). Lead preconcentration by solid phase extraction using oxidized carbon xerogel and spectrophotometric determination with dithizone. Microchem. J. *128*, 166–171.

Massoumi, B., Abbasian, M., Jahanban-Esfahlan, R., Mohammad-Rezaei, R., Khalilzadeh, B., Samadian, H., Rezaei, A., Derakhshankhah, H., and Jaymand, M. (2020). A novel bio- inspired conductive, biocompatible, and adhesive terpolymer based on polyaniline, polydopamine, and polylactide as scaffolding biomaterial for tissue engineering application. Int. J. Biol. Macromol. *147*, 1174–1184.

Naidoo, R., and Fisher, B. (2020). Sustainable development goals: Pandemic reset. Nature *583*, 198–201.

Oh, Y., Jeong, H., Lim, S., and Hong, J. (2020). Controlled nitric oxide release using poly(lactic-*co*- glycolic acid) nanoparticles for anti-inflammatory effects. Biomacromolecules *21*, 4972–4979.

Ortega, D.E., Matute, R.A., and Toro-Labbe, A. (2020). Exploring the nature of the energy barriers on the mechanism of the Zirconocene-catalyzed ethylene polymerization: a quantitative study from reaction force analysis. J. Phys. Chem. C *124*, 8198–8209.

Porfyris, A., Vasilakos, S., Zotiadis, C., Papaspyrides, C., Moser, K., Van der Schueren, L., Buyle, G., Pavlidou, S., and Vouyiouka, S. (2018). Accelerated ageing and hydrolytic stabilization of poly(lactic acid) (PLA) under humidity and temperature conditioning. Polym. Test. *68*, 315–332.

Puangprasert, S., and Prueksasit, T. (2019). Health risk assessment of airborne Cd, Cu, Ni and Pb for electronic waste dismantling workers in Buriram

Province. Thailand. J. Environ. Manag. *252*, 109601.

Rocca-Smith, J.R., Whyte, O., Brachais, C.H., Champion, D., Piasente, F., Marcuzzo, E., Sensidoni, A., Debeaufort, F., and Karbowiak, T. (2017). Beyond biodegradability of poly(lactic acid): physical and chemical stability in humid environments. ACS Sustain. Chem. Eng. *5*, 2751–2762.

Roytman, V.A., and Singleton, D.A. (2020). Solvation dynamics and the nature of reaction barriers and ion-pair intermediates in carbocation reactions. J. Am. Chem. Soc. *142*, 12865–12877.

Safi, J.M., Yassin, M.M., El-Nahhal, Y.Z., Abed, Y.A., Safi, M.J., and Suleiman, H.D. (2019). Childhood lead poisoning in Gaza strip, the Palestinian Authority. J. Trace Elem. Med. Biol. *54*, 118–125.

Sedghi, R., Heidari, B., and Behbahani, M. (2015). Synthesis, characterization and application of poly(acrylamide-*co*-methylenbisacrylamide) nanocomposite as a colorimetric chemosensor for visual detection of trace levels of Hg and Pb ions. J. Hazard. Mater. *285*, 109–116.

Sedghi, R., Kazemi, S., and Heidari, B. (2017). Novel selective and sensitive dual colorimetric sensor for mercury and lead ions derived from dithizone-polymeric nanocomposite hybrid. Sensor. Actuat. B *245*, 860–867.

Sherkhanov, S., Korman, T.P., Chan, S., Faham, S., Liu, H.J., Sawaya, M.R., Hsu, W.T., Vikram, E., Cheng, T., and Bowie, J.U. (2020). Isobutanol production freed from biological limits using synthetic biochemistry. Nat. Commun. *11*, 4292.

Shin, H.M., Ju, Y., Kim, G., Lee, J.W., Seo, M.W., Sim, J.H., Yang, J., Noh, S., Kim, J., and Kim, H.-R. (2019). Recyclable cytokines on short and injectable polylactic acid fibers for enhancing T-cell function. Adv. Funct. Mater. *29*, 1808361.

Silva Vinicius, A.O.P., Fernandes-Junior, W.S., Rocha, D.P., Stefano, J.S., Munoz, R.A.A., Bonacin, J.A., and Janegitz, B.C. (2020). 3D-printed reduced graphene oxide/polylactic acid electrodes: a new prototyped platform for sensing and biosensing applications. Biosens. Bioelectron. *170*, 112684.

Srivats, S., Zhang, D.M., Buffie, C., Wan, D., and Maltz, C. (2020). Poisoned by indian herbal medicine: an inconspicuous cause for abdominal pain. Am. J. Gastroenterol. *114*, 1506.

Stockmann, P.N., Van Opdenbosch, D., Poethig, A., Pastoetter, D.L., Hoehenberger, M., Lessig, S., Raab, J., Woelbing, M., Falcke, C., and Winnacker, M. (2020). Biobased chiral semi-crystalline or amorphous high-performance polyamides and their scalable stereoselective synthesis. Nat. Commun. *11*, 509.

Suda, Y., Arano, A., Fukui, Y., Koshida, S., Wakao, M., Nishimura, T., Kusumoto, S., and Sobel, M. (2006). Immobilization and clustering of structurally defined oligosaccharides for sugar chips: an improved method for surface plasmon resonance analysis of protein-carbohydrate interactions. Bioconjug. Chem *17*, 1125–1135.

Tahtat, D., Bouaicha, M.N., Benamer, S., Nacer-Khodja, A., and Mahlous, M. (2017). Development of alginate gel beads with a potential use in the treatment against acute lead poisoning. Int. J. Biol. Macromol. *105*, 1010–1016.

Torres, G.M., Liu, Y., and Arndtsen, B.A. (2020). A dual light-driven palladium catalyst: Breaking the barriers in carbonylation reactions. Science *368*, 318–323.

Wan, L., Li, C.X., Sun, C., Zhou, S., and Zhang, Y.H. (2019a). Conceiving a feasible degradation model of polylactic acid-based composites through hydrolysis study to polylactic acid/wood flour/polymethyl methacrylate. Compos. Sci. Technol. *181*, 107675.

Wan, L., Zhou, S., and Zhang, Y.H. (2019b). Parallel advances in improving mechanical properties and accelerating degradation to polylactic acid. Int. J. Biol. Macromol. *125*, 1093–1102.

Wang, C.C., Qin, X.L., Kan, J.Q., Liu, X., Suo, H.Y., and Zhong, J.F. (2021). Comparison of reactive sites of different fatty acid molecules: quantum chemistry calculation. Food Sci. https://doi.org/10.2206/TS.20200601.1434.062.

Wang, D., Cui, J.H., Gan, M.Z., Xue, Z.H., Wang, J., Liu, P.F., Hu, Y., Pardo, Y., Hamada, S., Yang, D.Y., and Luo, D. (2020a). Transformation of biomass DNA into biodegradable materials from gels to plastics for reducing petrochemical consumption. J. Am. Chem. Soc. *142*, 10114–10124.

Wang, J., Wang, H.Y., Mo, X.M., and Wang, H.J. (2020b). Reduced graphene oxide-encapsulated microfiber patterns enable controllable formation of neuronal-like networks. Adv. Mater. *32*, 2004555.

Wang, Z.-Y., Luo, Y.-F., Ye, R.-R., and Song, X.-M. (2011). Synthesis of novel biodegradable material poly(lactic acid-trimesic acid) *via* direct melt copolycondensation and its characterization. J. Polym. Res. *18*, 499–508.

Wang, Z.-Y., Zhao, H.-J., Wang, Q.-F., Ye, R.-R., and Finlow, D.E. (2010). Synthesis of poly(D,L-lactic acid) modified by cholic acid *via* direct melt copolycondensation and its characterization. J. Appl. Polym. Sci. *117*, 1405–1415.

Wang, Z.-Y., Zhao, Y.-M., Wang, F., and Wang, J. (2006). Syntheses of poly(lactic acid-*co*-glycolic acid) serial biodegradable polymer materials *via* direct melt polycondensation and their characterization. J. Appl. Polym. Sci. *99*, 244–252.

Xiong, C.D., Cheng, L.M., Xu, R.P., and Deng, X.M. (1991). Studies on the copolymerization of D,L-lactide with poly(tetramethylene ether glycol). J. Func. Polym. *4*, 133–138.

Xiong, J.-F., Wang, Q.-F., Peng, P., Shi, J., Wang, Z.-Y., and Yang, C.-L. (2014). Design, synthesis, and characterization of a potential flame retardant poly(lactic acid-*co*-pyrimidine-2,4,5,6-tetramine) *via* direct melt polycondensation. J. Appl. Poly. Sci. *131*, 40275.

Yan, Y.Z., Yang, S.L., Zhou, Y.J., Song, Y., Huang, J., Liu, Z.P., Wang, Y.B.N., and Wei, S. (2020). Estimating the national burden of mild intellectual disability in children exposed to dietary lead in China. Environ. Int. *137*, 105553.

Ye, S.F., and Neese, F. (2011). Nonheme oxo-iron(IV) intermediates form an oxyl radical upon approaching the C-H bond activation transition state. Proc. Nat. Acad. Sci. U S A *108*, 1228–1233.

Yuntawattana, N., McGuire, T.M., Durr, C.B., Buchard, A., and Williams, C.K. (2020). Indium phosphasalen catalysts showing high isoselectivity and activity in racemic lactide and lactone ring opening polymerizations. Catal. Sci. Technol. *10*, 7226–7239.

Zhang, Y., Huang, H., Liang, Z.L., Liu, H.H., Yi, L., Zhang, J.H., Zhang, Z.Q., Zhong, C., Huang, Y.G., and Ye, G.D. (2017). Microscopic progression in the free radical addition reaction: modeling, geometry, energy, and kinetics. J. Mol. Model. *23*, 73.

Zhao, Y.-M., Wang, Z.-Y., and Yang, F. (2005). Characterization of poly(D,L-lactic acid) synthesized by direct melt polymerization and its application in Chinese traditional medicine compound prescription microspheres. J. Appl. Polym. Sci. *97*, 195–200.

Zheng, Y., and Pan, P.J. (2020). Crystallization of biodegradable and biobased polyesters: Polymorphism, cocrystallization, and structure-property relationship. Prog. Polym. Sci. *109*, 101291.

Zhou, X.H., Zhou, J.J., Liu, Y.C., Guo, J., Ren, J.L., and Zhou, F. (2018). Preparation of iminodiacetic acid-modified magnetic biochar by carbonization, magnetization and functional modification for Cd(II) removal in water. Fuel *233*, 469–479.

Zimmerman, J.B., Anastas, P.T., Erythropel, H.C., and Leitner, W. (2020). Designing for a green chemistry future. Science *367*, 397–400.

Zou, X.J., Jie, J.Z., and Yang, B. (2017). Single-step enrichment of *N*-glycopeptides and phosphopeptides with novel multifunctional Ti^{4+}-immobilized dendritic polyglycerol coated chitosan nanomaterials. Anal. Chem. *89*, 7520–7526.

STAR★METHODS

KEY RESOURCES TABLE

REAGENT or RESOURCE	SOURCE	IDENTIFIER
Chemicals, peptides, and recombinant proteins		
D,L-Lactic acid (LA)	Guangzhou chemical reagent factory	CAS: 50-21-5
Iminodiacetic acid (IDA)	Energy chemical technology	CAS: 142-73-4
Dithizone	Energy chemical technology	CAS: 60-10-6
Deposited data		
Raw and analyzed data	This paper	N/A
Software and algorithms		
Materials Studio	Accelrys	www.accelrys.com

RESOURCE AVAILABILITY

Lead contact

Further requests for resources regarding this study will be fulfilled by the corresponding author, Zhaoyang Wang (wangzy@scnu.edu.cn).

Materials availability

This work did not produce any new unique reagents.

Data and code availability

All data are published in this manuscript and supplement; additional requests for data can be made by contacting the lead contact.

METHOD DETAILS

Materials

D,L-Lactic acid (LA), tin chloride ($SnCl_2$), stannous oxide (SnO), zinc chloride ($ZnCl_2$), zinc oxide (ZnO), and lead nitrate [$Pb(NO_3)_2$] were purchased from Guangzhou chemical reagent factory. Chloromethane ($CHCl_3$), anhydrous methanol (CH_3OH), and dimethyl sulfoxide (DMSO) were purchased from Tianjin Damao chemical reagent factory. Iminodiacetic acid (IDA) and dithizone were purchased from Energy chemical technology (Shanghai) Co. Ltd. All these reagents were used without further purification.

Theoretical computation

According to the method in literature (Ayers and Parr, 2000; Ye and Neese, 2011; Ortega et al., 2020), we made a theoretical computation for the possible reactions in the initial stage of polymerization. The geometric structures of LA and IDA molecules are optimized through the B3LYP function by Materials Studio, then the charge distribution is computed, and the possible reaction sites are analyzed. For different reaction modes that may occur at different sites, their transition states and energy barriers are calculated and searched, respectively, which provides a theoretical basis for the synthesis process, as well as the structure and performance analysis (Lu and Manzetti, 2014; Gorantla and Mallik, 2020; Zhang et al., 2017).

Synthesis of copolymers

According to our previous works (Lin et al., 2020; Luo et al., 2017), LA and IDA were stirred for 4 h at 140 °C under normal pressure for dehydration, and prepolymerized for 4 h at 140 °C under 10 kPa pressure in a flask. Then, the reaction system was heated with an electromagnetic stirring heater and vacuumed with a rotary vane vacuum pump. Once the catalyst was added in a certain percentage by weight of the prepolymer (*wt*%), and the direct melt polycondensation was carried out under a specified temperature and 5 kPa pressure for a certain time. The product was purified by methanol and deionized water and dried in a vacuum dryer at 45 °C for 48 h, then ground into powder.

Structure characterization

The Fourier transform infrared spectroscopy (FTIR) of copolymers was recorded by infrared spectrometer (Spectrum Two, Perkin Elmer, America) using a potassium bromide tableting method. The ^{1}H NMR spectra of copolymers were detected by NMR spectrometer (DRX-600, Varian, America) in $CDCl_3$ solution and using TMS as internal standard at 600 MHz. The relative molecular weight of copolymers was determined by gel permeation chromatography (GPC, P230II, Elitehplc, China) with $CHCl_3$ as solvent at 25 °C and a flow velocity of 1 mL·min^{-1}.

Tests of physical properties

The intrinsic viscosity ([η]) of copolymers was determined with an Ubbelohde viscometer using chloroform as solvent at 25±0.1 °C in a constant temperature water bath (Lin et al., 2020; Luo et al., 2019). The diffraction patterns of copolymers were obtained by X-ray diffractometer (XRD, X'Pert PRO, Panalytical, Netherlands). The glass transition temperature (T_g) of copolymers was measured by differential scanning calorimeter (DSC, TA-60WS, Shimadzu, Japan) with the test temperature range from -20 °C to 180 °C and the heating rate of 10 °C·min^{-1}. The thermal stability of copolymers was measured by thermogravimetric analyzer (TG, 209 F3, Netzsch, Germany) in the temperature range from 50 °C to 800 °C, at the heating rate of 10 °C·min^{-1}, the oxygen flow rate of 10 mL·min^{-1}, and the nitrogen flow rate of 40 mL·min^{-1}.

Degradation test

Referring to the literature (Wan et al., 2019a, 2019b), the appropriate degradation conditions in this work were set as follow. The weight of empty reaction flask is recorded as W_b, and the total weight of flask and sample is recorded as W_a. After adding 20 mL of deionized water, the flask with sample was sealed. Then, it was put into a 37 °C constant temperature water bath for degradation, and fully shaken every 24 h. At the time of the pre-planned degradation cycle, such as 1, 2, 3 and 4 weeks, respectively, the corresponding flasks were taken out and centrifuged at 4000 rpm for 10 min. After the supernatant was poured, the precipitate was washed with deionized water. The process of centrifugation and pouring supernatant was repeated for several times. Then, the flasks were dried in a vacuum dryer at 45 °C for 48 h, the total weight of flask and undegraded sample was recorded as W_d. The degradation rate (R_d) was calculated according to the formula: $R_d = (W_a - W_d) / (W_a - W_b)$.

Lead ion chelating test

As reported in the literatures (Sedghi et al., 2015, 2017; Maratta et al., 2016), the chelating test for lead ion was accorded the method in the following. A pH neutral solution of $Pb(NO_3)_2$ with 2 mg·L^{-1} Pb^{2+} as original standard and working solution was prepared. And 5 mg·L^{-1} dithizone ethanol solution as the complexing agent and the indicator for its complexing reaction with Pb^{2+} was prepared also. The standard solutions of $Pb(NO_3)_2$ with gradient concentration, such as 0.2, 0.5, 0.8, 1.0, 1.2, 1.5, and 1.8 mg·L^{-1} were prepared by its 2 mg·L^{-1} original standard solution. Then, they respectively with dithizone ethanol solution as a volume ratio of 1:1 were added into a colorimetric dish. Once the UV-*vis* absorption value of the mixtures was measured (UV-2700, Shimadzu, Japan), the standard curve of concentration-absorption value was made.

After the addition of 100 mL of Pb^{2+} working solution and 250 mg of P(LA-*co*-IDA) samples, the chelating flasks were placed in a 37 °C constant temperature water bath to degrade the samples, release IDA and form IDA-Pb chelate. When the degradation-chelation reaction time was 1, 2, 3 and 4 weeks, 2 mL of working solution was drawn from the flasks, and 2 mL of deionized water was added into the flasks. The degradation-chelation solution and dithizone ethanol solution were added into a colorimetric dish as a volume ratio of 1:1, and the UV-*vis* absorption value of the mixtures was measured. To characterize the capacity of P(LA-*co*-IDA) on Pb^{2+}, the UV-*vis* absorption value was substituted into the linear fitting equation of the standard curve. Thus, the concentration of the remaining unchelated Pb^{2+} in the degradation-chelation solution was obtained (Sedghi et al., 2015).

QUANTIFICATION AND STATISTICAL ANALYSIS

All the [η] in polymerization condition screening experiments were tested in triplicate, data were shown in Table 1. Statistical differences were determined by square difference. $P < 0.05$ was considered statistically significant. The statistical analyses were performed with Statistical Product and Service Solutions software (SPSS).

ADDITIONAL RESOURCES

There is no additional resources need to be declared in this manuscript, additional requests for this can be made by contacting the lead contact.